

## ESI for “Hydrogen Bonding-Assisted Thermal Conduction in $\beta$ -Sheet Crystals of Spider Silk Protein”

Lin Zhang,<sup>a</sup> Teli Chen,<sup>b</sup> Heng Ban,<sup>a</sup> and Ling Liu<sup>a\*</sup>

<sup>a</sup> *Department of Mechanical and Aerospace Engineering, Utah State University, Logan, UT  
84322, USA*

<sup>b</sup> *The Newman School, Boston, MA 02116, USA*

**S1. Structure**

**S2. Determination of Unit Cell Size**

**S3. Determination of Area**

**S4. Representative Temperature Profile and Determination of  $\frac{dT}{dx}$**

**S5. Phonon Density of States (DOS) and Partial DOS Profiles for Representative  $\beta$ -Sheet Structures**

---

\* Email: [ling.liu@usu.edu](mailto:ling.liu@usu.edu)

## S1. Structure

This study is focused on poly-A  $\beta$ -sheet because according to experiment, the  $\beta$ -sheet is an important component of *N. Clavipes* spider silk [Figure S1(a)]. The atomistic structure of poly-A  $\beta$ -sheet was built based on previous work that simulates the mechanical response of poly-A  $\beta$ -sheets [1]. Our  $\beta$ -sheet models were verified by visualization with the Visual Molecular Dynamics (VMD) package [2]. A snapshot from VMD [Figure S1(b)] shows that hydrogen bonds (red lines) are spontaneously formed in the equilibrated  $\beta$ -sheet structure.

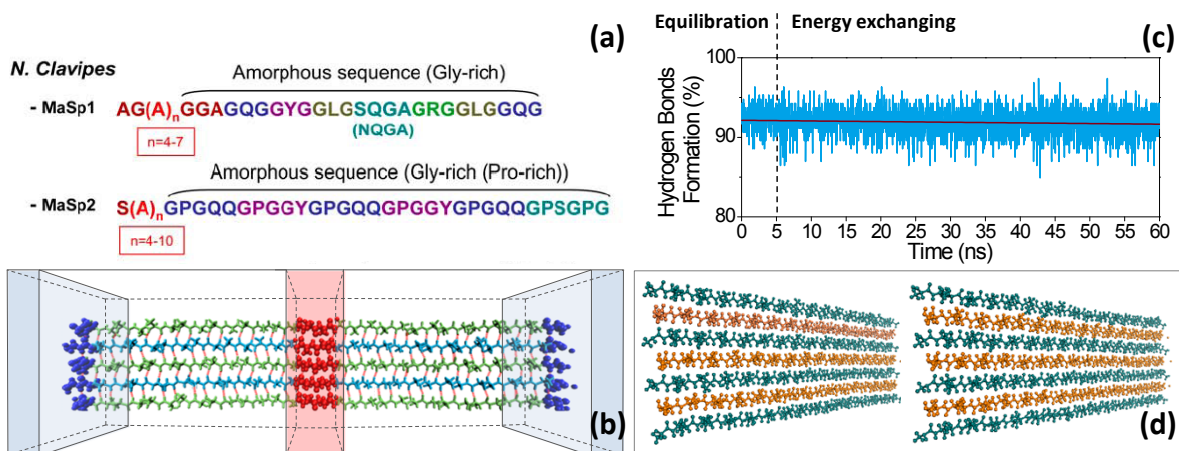


Figure S1. (a) Protein sequence of MaSp1 and MaSp2 *N. Clavipes* spider silk [3]. (b) A snapshot of the simulation model from VMD. (c) Percentage of hydrogen bond formation versus simulation time. (d) Structural comparison between a  $\beta$ -sheet right after equilibration and the same  $\beta$ -sheet in steady-state energy exchange.

To demonstrate the stability of hydrogen bonds in our models, Figure S1(c) plots the *percentage of hydrogen bond formation* versus simulation time. The percentage of hydrogen bond formation is calculated by taking a ratio between the number of hydrogen bonds at any time instant and the number of hydrogen bonds that could be formed in the ideal condition. Results show that the percentage of hydrogen bond formation remains  $\sim 91\%$  during the equilibration and the energy exchange procedures. VMD snapshots in Figure S1(d) show that the structure does not change much either. The insensitivity of protein structure to energy exchange is due to the very careful procedure we followed when performing the research. The frequency of energy exchange was fine-tuned for all jobs such that the temperature difference between the two ends of the protein is about  $30 \pm 2$  K. The temperature difference is small enough to avoid protein denaturation at high temperatures [4]. It is also large enough to overcome thermal perturbation such that smooth temperature profiles could be obtained.

We note that molecular dynamics simulation does not require the identification of hydrogen bonds. However, we need to identify hydrogen bonds in the visualization and analysis processes, e.g. Figure S1(b,c). Although there are several different geometric definitions of hydrogen bonds available [5,6], we employed a widely adopted criterion [7] by which hydrogen bond is defined when the distance between the donor (D) and the acceptor (A) is less than 3.5 Angstrom, and the angle of ADH is less than 30 degree (H represents the hydrogen atom). Using different criteria could give slightly different numbers of hydrogen bonds. However, this would not affect any simulation result because molecular dynamics simulation does not involve the identification of hydrogen bonds. This would not significantly affect visualization and analysis [e.g. Figure S1(b,c)] either because the physics is not changed.

## S2. Determination of Unit Cell Size

Stress state plays a key role in thermal transport [8-10]. In the present work, we attempted to make the model under a free stress state. We also attempted to make it not floppy in the length direction so that there was no transverse expansion and oscillation. The model generated this way enabled us to focus on the intrinsic effects of hydrogen bonding on thermal transport.

The desired model was generated by choosing an appropriate unit cell size in the length direction. Theoretically, when the unit cell size is too small, transverse expansion would happen. This will (1) break some of the hydrogen bonds, and (2) increase potential energy due to forced bending of the  $\beta$ -sheet. Similarly, when the unit cell size is too large, the  $\beta$ -sheet would be stressed, increasing potential energy and breaking some of the hydrogen bonds.

Therefore, at the “appropriate” unit cell size, system potential energy should minimize and the number of hydrogen bonds should maximize. Figure S2 shows the variations of potential energy and the number of hydrogen bond as functions of the unit cell size along the length direction. To be clear, the unit cell size is normalized by the size adopted for this research, 0.396 nm per residue. It is shown that potential energy minimizes and the number of hydrogen bond maximizes at the chosen unit cell size. This demonstrates that the structures adopted in this research are free from significant stress and transverse expansion. This is also evidenced by the snapshots shown in Figure S1(b,d) where no transverse expansion is observed.

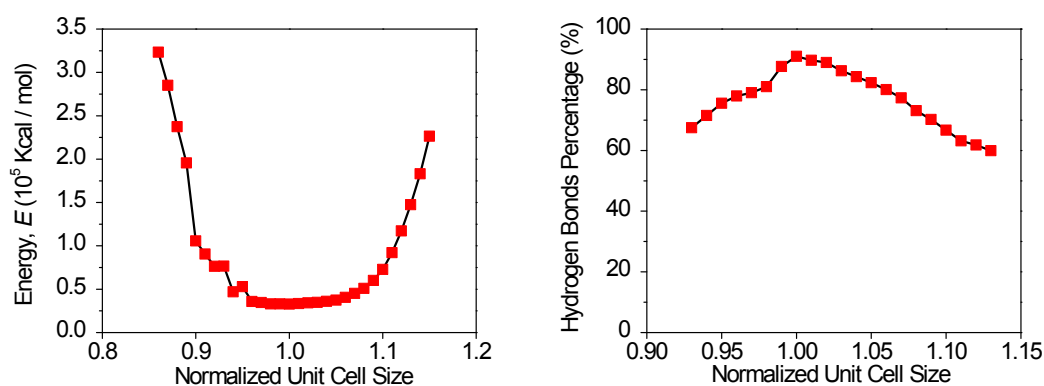


Figure S2. Variations of (a) system potential energy and (b) number of hydrogen bonds with respect to unit cell size along the length direction. The horizontal axes are normalized by the currently adopted unit cell size, 0.396 nm per residue. When the normalized unit cell size is larger than 1, the  $\beta$ -strands are stressed under tension. When the normalized unit cell size is smaller than 1, the  $\beta$ -strands are sloppy leading to transverse expansion.

### S3. Determination of Area

Thermal conductivity calculation involves a critical parameter – area. The determination of the area (or thickness) of low-dimensional materials (e.g. graphene and carbon nanotube) has been an active research topic for several years. Many previous papers studying the thermal properties of graphene have used the thickness of 0.335 nm [11,12]. This represents a common approach to obtain the thickness of graphene – consider graphene as a uniform slab in graphite and adopt the interlayer spacing in graphite as the thickness of graphene. There are also several other ways to determine the graphene thickness, but most of them give consistent results [13].

For  $\beta$ -strands, we adopted an approach similar to that commonly used for graphene. First, a block of  $\beta$ -strands (Figure S3b) were generated and equilibrated for 20 ns. Snapshots were generated every 10ps during the last 10 ns simulation. Each snapshot gave a “lattice” formed by the interior 25  $\beta$ -strands (Figure S3c). Lattice parameters were then averaged to achieve the area associated with each  $\beta$ -strand. Averaging over the 1000 snapshots led to a value of 0.236 nm<sup>2</sup>, which was used in all the thermal conductivity calculations presented in this work.

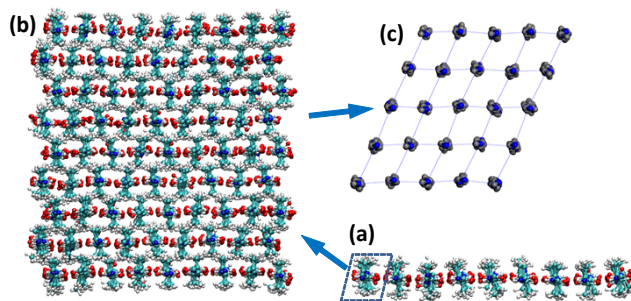


Figure S3. Determination of the area associated with each  $\beta$ -strand: (a) a  $\beta$ -sheet consisting of 9  $\beta$ -strands; (b) a block of  $\beta$ -strands (9 layers of 9-strand  $\beta$ -sheets, totaling 81  $\beta$ -strands); (c) The “lattice” formed by the interior 5x5  $\beta$ -strands. The area associated with each  $\beta$ -strand is an average over the 25  $\beta$ -strands during a 10 ns simulation.

#### S4. Representative Temperature Profile and Determination of $\frac{dT}{dx}$

Thermal conductivity calculation also involves another critical parameter –  $\frac{dT}{dx}$ , which should be determined by molecular simulations under the Muller-Plathe framework. Figure S4 shows the variation of temperature along the length direction of an A16-7-1  $\beta$ -sheet. The  $\beta$ -sheet was divided into 16 slabs for evaluating temperature. The curve is nonlinear. Previous applications of the Muller-Plathe method [14-19] suggested using the relatively linear region in the curve to evaluate  $\frac{dT}{dx}$ . In this work, only the temperature for slabs 5-13 were used to fit  $\frac{dT}{dx}$ .

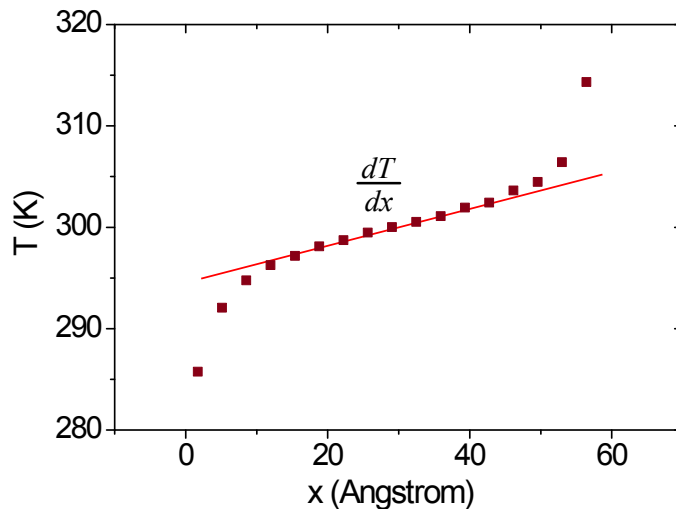


Figure S4. Determination of  $\frac{dT}{dx}$ . Temperature profile is evaluated along the length direction ( $x$ ).

## S5. Phonon Density of States (DOS) and Partial DOS Profiles for Representative $\beta$ -Sheet Structures

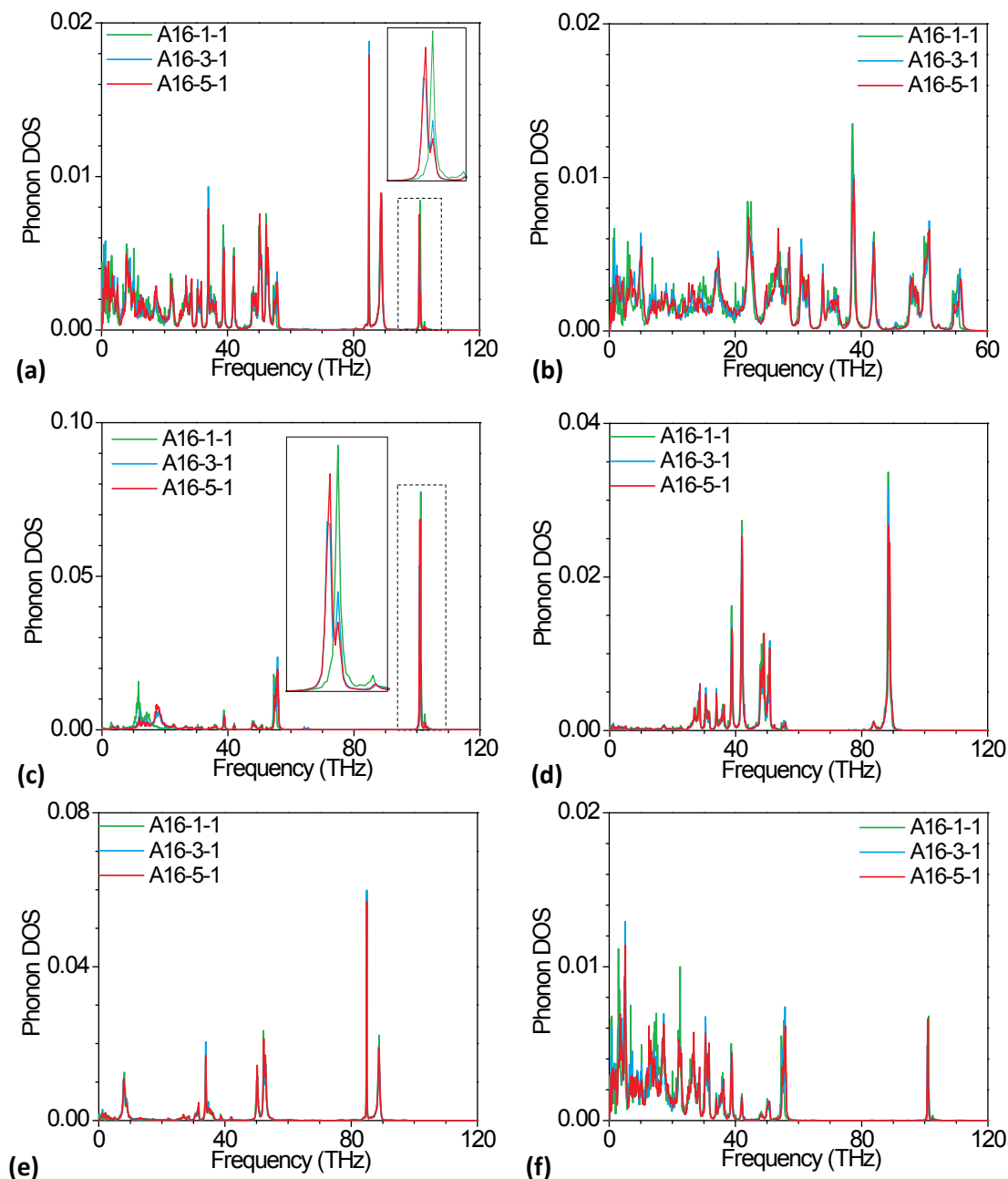


Figure S5. (a) Phonon DOS profiles of three anti-parallel  $\beta$ -sheet structures (A16-1-1, A16-3-1, and A16-5-1). Partial phonon DOS projected on (b) backbone atoms, (c) H atoms (hydrogen atoms bonded to nitrogen atoms), (d) HA atoms (hydrogen atoms bonded to  $\alpha$ -carbon atoms), (e) HB atoms (hydrogen atoms of methyl groups), and (f) nitrogen atoms (denoted by N). (a) and (b) show that phonon spectra of A16-3-1 and A16-5-1 are close to each other, but different from that of A16-1-1. The inset of (c) shows that frequency of phonons corresponding to vibration of H atoms shifts from 101.2 to 100.8 THz due to hydrogen bonding. (d) and (e) demonstrate that primary phonon modes of HA and HB have the frequency of 88.6 and 84.8 THz, respectively. (f) shows a blue shift in the frequency of the phonon mode of N atoms in low-frequency regime, from A16-1-1 to A16-3-1 and A16-5-1.

## References

- [1] S. B. Xiao, W. Stacklies, M. Cetinkaya, B. Markert, and F. Grater, *Biophys J* **96**, 3997 (2009).
- [2] W. Humphrey, A. Dalke, and K. Schulten, *Journal of Molecular Graphics* **14**, 33 (1996).
- [3] T. Lefèvre, M.-E. Rousseau, and M. Pézolet, *Biophys J* **92**, 2885 (2007).
- [4] D. Paschek and A. E. Garcia, *Phys Rev Lett* **93**, 238105 (2004).
- [5] T. Steiner, *Angewandte Chemie International Edition* **41**, 48 (2002).
- [6] R. Taylor, O. Kennard, and W. Versichel, *Acta Crystallogr. Sect. B-Struct. Commun.* **40**, 280 (1984).
- [7] A. Luzar and D. Chandler, *Nature* **379**, 55 (1996).
- [8] J. Zhang *et al.*, *Sensors* **13**, 9388 (2013).
- [9] W. Ning, X. Lanqing, W. Hui-Qiong, and Z. Jin-Cheng, *Nanotechnology* **22**, 105705 (2011).
- [10] K. Jung, M. Cho, and M. Zhou, *Journal of Applied Physics* **112** (2012).
- [11] J. Hu, X. Ruan, and Y. P. Chen, *Nano Letters* **9**, 2730 (2009).
- [12] Y. Ni, Y. Chalopin, and S. Volz, *Applied Physics Letters* **103** (2013).
- [13] W. Philipp, V. I. Viktoria, J. R. Mark, R. B. Patrick, and P. E. Christopher, *Journal of Physics: Condensed Matter* **25**, 155302 (2013).
- [14] E. Lussetti, T. Terao, and F. Müller-Plathe, *The Journal of Physical Chemistry B* **111**, 11516 (2007).
- [15] T. Terao, E. Lussetti, and F. Müller-Plathe, *Physical Review E* **75**, 057701 (2007).
- [16] E. Rossinsky and F. Müller-Plathe, *The Journal of Chemical Physics* **130** (2009).
- [17] E. A. Algaer, M. Alaghemandi, M. C. Böhm, and F. Müller-Plathe, *The Journal of Physical Chemistry A* **113**, 11487 (2009).
- [18] N. Boris, W. Taku, and R. P. Simon, *Journal of Physics: Condensed Matter* **21**, 084219 (2009).
- [19] P. K. Schelling, S. R. Phillpot, and P. Keblinski, *Physical Review B* **65**, 144306 (2002).